

## Self-Assembled Monolayers of Alkaneselenolates on (111) Gold and Silver

A. Shaporenko,<sup>†</sup> A. Ulman,<sup>‡,||</sup> A. Terfort,<sup>§</sup> and M. Zharnikov<sup>\*,†</sup>

Angewandte Physikalische Chemie, Universität Heidelberg, Im Neuenheimer Feld 253, 69120 Heidelberg, Germany, Department of Chemical and Biological Sciences and Engineering, Polytechnic University, Six Metrotech Center, Brooklyn, New York, and Anorganische und Angewandte Chemie, Universität Hamburg, 20146 Hamburg, Germany

Received: October 29, 2004; In Final Form: December 27, 2004

Self-assembled monolayers (SAMs) formed from didodecyl diselenide (C12SeSeC12) and didodecyl selenide (C12SeC12) on (111) Au and Ag substrates were extensively characterized by several complementary techniques. C12SeSeC12 was found to form contamination-free, densely packed, and well-ordered C12Se SAMs on both substrates, whereas the adsorption of C12SeC12 occurred only on Au and resulted in the formation of a SAM-like C12SeC12 film with a low packing density and a conformational disorder. The properties of the C12Se SAMs were compared with those of dodecanethiolate (C12S) SAMs. The packing density, orientational order, and molecular inclination in C12Se/Au and C12S/Au were found to be very similar. In contrast, C12Se/Ag exhibited significantly lower packing density, a lower degree of the conformational and orientational order, and a larger molecular inclination than C12S/Ag. The results suggest a  $sp^3$  bonding configuration for the selenium atom on Au and Ag and indicate a larger corrugation of the headgroup–substrate binding energy surface in C12Se/Ag than in C12S/Ag.

### 1. Introduction

Frontier areas of modern technology rely on the possibility to tailor surface properties such as wetting, adhesion, lubrication, corrosion, and biocompatibility both on microscopic and macroscopic scales. To a definite extent, this possibility is provided by self-assembled monolayers (SAMs), which are 2D polycrystalline films of semirigid molecules that are chemically anchored to a suitable substrate.<sup>1–5</sup> So far, the focus SAM systems were films of *n*-alkanethiolates (AT) on (111) gold and silver substrates.<sup>3,4</sup> These films have been used and are still being used both as an archetypal system to investigate the properties and behavior of SAMs as well as an efficient platform for several applications.<sup>3–5</sup> It is well-known that the properties of AT/Au and AT/Ag are rather different, what is mainly related to the different corrugations of the sulfur–gold and sulfur–silver binding energy surfaces.<sup>1–3,6</sup> In case of Ag, this corrugation is relatively weak, which allows a dense packing of AT chains in a  $(\sqrt{7} \times \sqrt{7})R19.1^\circ$  incommensurate structure with a lattice constant of  $\approx 4.67$ – $4.77$  Å, close to the next neighbor distance in bulk paraffin or polyethylene crystals ( $\approx 4.4$  Å).<sup>2,4,7–9</sup> In the case of Au, the corrugation of the sulfur–metal potential is assumed to be more pronounced,<sup>6</sup> which results in the formation of a nearly commensurate  $c(4 \times 2)$ -modulated  $(\sqrt{3} \times \sqrt{3})R30^\circ$  lattice, with a larger intermolecular spacing of  $\approx 5.0$  Å.<sup>2,4,7,10,11</sup> In this lattice, minimization of energy is achieved by tilting of the AT molecules by  $\approx 30^\circ$  (the measured tilt angle depends on the experimental technique used<sup>12</sup>),<sup>10,13,14</sup> which is noticeably larger than the tilt in the AT/Ag systems ( $10$ – $12^\circ$ ).<sup>8,14</sup> Along with the corrugation of the sulfur–substrate

binding energy surface, the bonding configuration of the chemisorbed sulfur headgroup is of importance, being  $sp^3$  and  $sp$  on Au(111) and Ag(111), respectively.<sup>14–20</sup> In general, the headgroup–substrate bond is the deciding factor in the balance of structural forces in aliphatic SAMs on metal substrates. By varying the character of this bond one can probably change the properties of these films to a noticeable extent and create novel systems, which can be of interest for applications. A straightforward way to do so is to use another headgroup than thiol, e.g. selenol.

The chemical properties of sulfur and selenium are quite similar. Both elements have the same valence electron configurations and are neighbors in the VIB column of the periodic table. A noticeable difference between them is, however, the van der Waals radius, which is 1.85 Å in the case of S and 2.0 Å in the case of Se. Despite the similarities, there has been, however, relatively little work done on selenol-derived SAMs,<sup>21–30</sup> including only few publications on alkaneselenols, and only on gold substrate.<sup>21,26,27,29</sup> Samant et al.<sup>21</sup> studied a SAM formed from docosaneselenolate (C22Se) SAM on Au(111) by surface X-ray diffraction. They found an incommensurate structure with an oblique unit cell, stated the average tilt angle of the alkyl chains as  $15^\circ$ , and postulated that the selenium–gold bond is weaker than the sulfur–gold one. Nakano et al.<sup>26</sup> used infrared spectroscopy, X-ray photoelectron spectroscopy (XPS), electrochemistry measurements, and a quartz-crystal microbalance to characterize decaneselenolate (C10Se) SAM on Au(111). They have concluded that decaneselenol adsorbs on Au surfaces to form stable monolayers as alkanethiols, with a similar packing density. Yee et al.<sup>27</sup> studied the functionalization of gold nanoparticles by didodecyl diselenide and found that AT chains pack more orderly on gold than their selenolate analogues. The binding energy of the Au–Se bond was found to be slightly higher than that of the Au–S bond, which is in a contradiction with the above statement of Samant et al.<sup>21</sup> Very

\* Corresponding author. E-mail: Michael.Zharnikov@urz.uni-heidelberg.de.

<sup>†</sup> Universität Heidelberg.

<sup>‡</sup> Polytechnic University.

<sup>§</sup> Universität Hamburg.

<sup>||</sup> Present address: Department of Chemistry, Bar-Ilan University, Ramat Gan 52900, Israel 2.

recently, Monnell et al.<sup>29</sup> characterized SAMs formed from didodecyl and didodecyl diselenides on Au(111) by scanning tunneling microscopy and found that the densely packed phase of the alkyl selenides is distorted hexagonal and incommensurate to the underlying gold substrates. The respective lattice constants were found to be very close to the previously reported X-ray diffraction values.<sup>21</sup>

In the present work we make a first attempt to compare the properties of alkaneselenolate SAMs on (111) Au and Ag substrates and perform an extended characterization of SAMs formed from didodecyl diselenide (C12SeSeC12), didodecyl selenide (C12SeC12), and dihexadecyl diselenide (C16SeSeC16) on these substrates. We used several complementary experimental techniques, including high-resolution XPS, near-edge X-ray absorption fine structure (NEXAFS) spectroscopy, infrared reflection absorption spectroscopy (IRRAS), ellipsometry, and contact angle measurements. The results for the C12SeSeC12 SAMs are presented to the full extent, whereas only some data and only a general description are given for the C12SeC12 and C16SeSeC16 films, respectively, which is related to their poor quality. As a direct reference for the alkaneselenolate films we used dodecanethiolate (C12S) SAMs on (111) Au and Ag.

In the following section we describe the experimental procedure and techniques. The results are presented and briefly discussed in section 3. An extended analysis of the data is given in section 4 followed by a summary in section 5.

## 2. Experimental Section

C12SeSeC12 and C12SeC12 were synthesized by refluxing Na<sub>2</sub>Se<sub>2</sub> (C12SeSeC12) or Na<sub>2</sub>Se (C12SeC12) with C<sub>12</sub>H<sub>25</sub>Br in ethanol. The product was purified by chromatography on SiO<sub>2</sub> using hexane as the eluent. The purified substance was crystallized from a mixture of 2-propanol and heptane. The synthesis of C16SeSeC16 was performed using the method described in ref 31, followed by a chromatographic purification using hexanes on silica. The resulting yellowish solid was obtained in quantitative yield. Its melting point of 46–48 °C was close to a literature value of 50–51 °C.<sup>32</sup> The substance turned out to be sensitive to light. C<sub>12</sub>H<sub>25</sub>SH (C12SH) was purchased from Sigma-Aldrich.

The gold and silver substrates were prepared by thermal evaporation of 200 nm of gold or 100 nm of silver (99.99% purity) onto mica or polished single-crystal silicon (100) wafers (Silicon Sense) primed with a 5 nm titanium adhesion layer. Such evaporated films are standard substrates for thiol-derived SAMs. They are polycrystalline, with a grain size of 20–50 nm as observed by atomic force microscopy. The grains predominantly exhibit a (111) orientation.<sup>33,34</sup> The SAMs were formed by immersion of freshly prepared substrates into a 5 μmol C12SeSeC12, C12SeC12, or C16SeSeC16 solution in absolute ethanol at room temperature for 24 h. After immersion, the samples were carefully rinsed with pure ethanol, blown dry with argon, and kept for several days in argon-filled glass containers until the characterization. No evidence for impurities or oxidative degradation products was found. Note that a μmol concentration and ethanol as the solvent were found to be crucial for the film quality. A millimolar concentration, used frequently for AT SAMs, resulted in poor-quality films. We have also tried some other solvents instead of ethanol (tetrahydrofuran, etc.), but this led to poor-quality films, as well.

For most of the experiments, we used SAMs formed from C12SH, as a direct reference to the selenium-derived films. The C12S SAMs were prepared by immersion of freshly prepared Au and Ag substrates into a 1 mmol C12SH solution in absolute

ethanol at room temperature for 24 h. The same cleaning and sample storage procedure as for the selenium-derived films was used.

The fabricated films were characterized by synchrotron-based HRXPS, XPS (data not shown, since HRXPS is superior), angle-resolved NEXAFS spectroscopy, Fourier transform IRRAS, ellipsometry, and contact angle measurements. All experiments were performed at room temperature. The HRXPS, XPS, and NEXAFS measurements were carried out under UHV conditions at a base pressure better than  $1.5 \times 10^{-9}$  mbar. The spectra acquisition time was selected in such a way that no noticeable damage by the primary X-rays occurred during the measurements.<sup>35–38</sup>

HRXPS experiments were performed at the bending magnet beamline D1011 at the MAX II storage ring of the MAX-lab synchrotron radiation facility in Lund, Sweden. For these measurements, only the films on mica were used. The HRXPS spectra were collected in normal emission geometry at photon energies of 150 eV for the Se 3d range, 350 and 580 eV for the C 1s range, and 350 eV for the S 2p region. In addition, Au 4f and Ag 3d spectra were acquired and the O 1s range was monitored. The binding energy (BE) scale of every spectrum was individually calibrated using the Au 4f<sub>7/2</sub> emission line of AT-covered Au substrate at 83.95 eV. The latter value is given by the latest ISO standard.<sup>39</sup> It is very close to a value of 83.93 eV, which has been obtained by us for Au 4f<sub>7/2</sub> using a separate calibration to the Fermi edge of a clean Pt-foil.<sup>34</sup> The energy resolution was better than 100 meV, which is noticeably smaller than the full widths at half-maximum (fwhm) of the photoemission peaks addressed in this study.

HRXPS spectra were fitted by symmetric Voigt functions and either a Shirley-type or linear background. To fit the Se 3d<sub>5/2,3/2</sub> and S 2p<sub>3/2,1/2</sub> doublets we used a pair of such peaks with the same fwhms, the branching ratios of 3:2 (3d<sub>5/2</sub>/3d<sub>3/2</sub>) and 2:1 (2p<sub>3/2</sub>/2p<sub>1/2</sub>), and spin-orbit splittings (verified by fit) of ≈0.86 eV (3d<sub>5/2</sub>/3d<sub>3/2</sub>) and ≈1.18 eV (2p<sub>3/2</sub>/2p<sub>1/2</sub>).<sup>40</sup> The fits were carried out self-consistently: the same peak parameters were used for identical spectral regions. The accuracy of the resulting BE/fwhm values is 0.02–0.03 eV.

NEXAFS spectroscopy measurements were performed at the HE-SGM beamline of the synchrotron storage ring BESSY II in Berlin, Germany. The spectra acquisition was carried out at the C K-edge in the partial electron yield mode with a retarding voltage of –150 V. Linear polarized synchrotron light with a polarization factor of ≈82% was used. The energy resolution was ≈0.40 eV. The incidence angle of the light was varied from 90° (*E*-vector in surface plane) to 20° (*E*-vector near surface normal) in steps of 10–20° to monitor the orientational order in the SAMs.

Raw NEXAFS spectra were normalized to the incident photon flux by division through a spectrum of a clean, freshly sputtered gold sample. In the case of Ag substrate, a spectrum of clean silver was subtracted from the raw spectrum of a SAM sample before the normalization.<sup>17,41</sup> The photon energy (PE) scale was referenced to the pronounced π<sub>1</sub>\* resonance of highly oriented pyrolytic graphite at 285.38 eV.<sup>42</sup>

IRRAS measurements were performed with a dry-air-purged Bio-Rad FTIR spectrometer Model FTS 175C equipped with a liquid nitrogen-cooled MCT detector. All spectra were taken using p-polarized light incident at a fixed angle of 80° with respect to the surface normal. The spectra were measured at a resolution of 2 cm<sup>-1</sup> and are reported in absorbance units  $A = -\log R/R_0$ , where *R* is the reflectivity of the substrate with the monolayer and *R*<sub>0</sub> is the reflectivity of the reference. Substrates

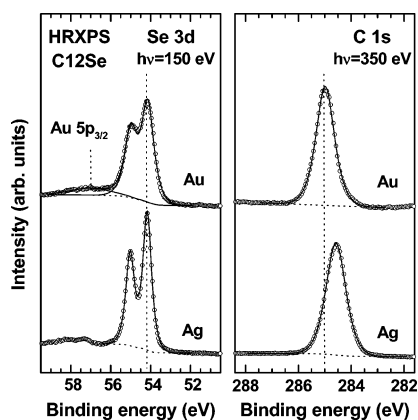


**Figure 1.** Normalized Se 3d and C 1s HRXPS spectra of C12Se/Au and C12Se/Ag (open circles) acquired at photon energies of 150 and 350 eV, respectively, along with the corresponding fits (solid lines). The BE positions of the Se 3d<sub>5/2</sub> component and C 1s emission for C12Se/Au are marked by the dotted lines. A background is shown.

covered with a perdeuterated hexadecanethiolate SAM were used as a reference.

Ellipsometry measurements were carried out using the M-44 ellipsometer of J. A. Woollam Co. Inc. The data were analyzed with the respective software. The incident angle was set to 75° and calibrated with a silicon wafer as a reference. A refractive index of 1.45 was assumed for all films in the calculation of their thickness.<sup>43,44</sup>

Advancing contact angles of Millipore water were measured on freshly prepared samples with a Krüss goniometer Model G1. The measurements were performed under ambient conditions with the needle tip in contact with the drop. At least three measurements at different locations on each sample were made. The averaged values are reported. Deviations from the average were less than ±1°.

### 3. Results

**3.1. HRXPS.** Normalized Se 3d and C 1s HRXPS spectra of C12Se/Au and C12Se/Ag are presented in Figure 1, along with the corresponding fits (we will use the abbreviation C12Se for the films formed from C12SeSeC12). The results of fitting and a quantitative analysis of these spectra are shown in Table 1, along with the analogous data for the C12SeC12 and C12S films (see below). The Se 3d spectra of both C12Se/Au and C12Se/Ag exhibit a single Se 3d<sub>5/2,3/2</sub> doublet, accompanied by a weak Au 5p<sub>3/2</sub> emission. The BE position of this doublet (54.15 eV) is distinctly different from that for the bulk C12SeSeC12 (55.3 eV),<sup>27</sup> suggesting that upon the adsorption of C12SeSeC12 on Au and Ag, the covalent Se–Se bonds are cleaved, through an oxidative addition mechanism, and selenolate-metal bonds are formed. Note, that there is a similar difference between the BE positions of the S 2p doublet in nonbound ATs and AT SAMs on noble metal substrates. As follows from Figure 2, where S 2p and C 1s spectra of C12S/Au and C12S/Ag are depicted, the BE position of the thiol-related doublet is close to 162.00 eV (see Table 1 for the exact values), whereas this energy for nonbound ATs is around 163.5 eV.<sup>45–48</sup>

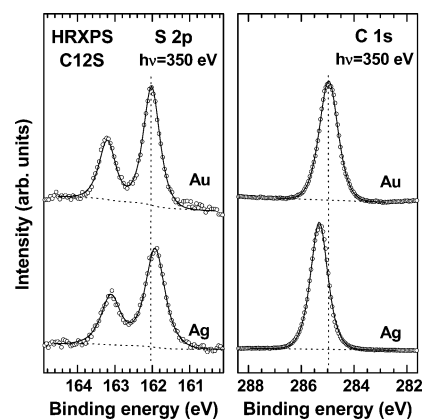


**Figure 2.** Normalized S 2p and C 1s HRXPS spectra of C12S/Au and C12S/Ag (open circles) acquired at a photon energy of 350 eV, along with the corresponding fits (solid lines). The BE positions of the S 2p<sub>3/2</sub> component and C 1s emission for C12S/Au are marked by the dotted lines. A background is shown.

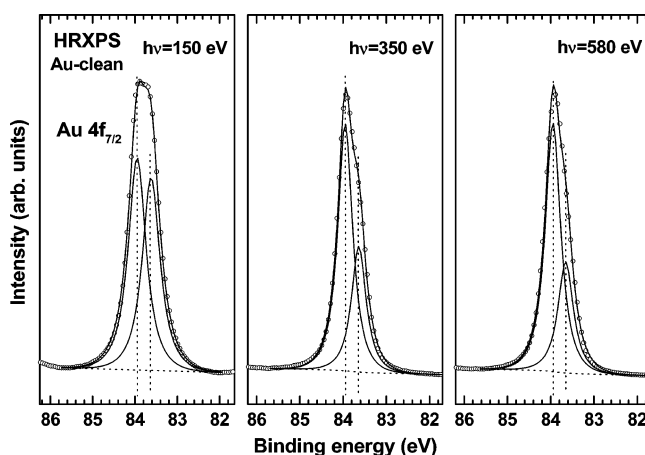


**Figure 3.** Normalized Au 4f<sub>7/2</sub> HRXPS spectra of clean Au acquired at photon energies of 150, 350, and 580 eV. The decomposition of the spectra into the bulk and surface components is shown.

In addition to the spectra of the headgroup (Se 3d), the building of the selenolate–metal bond can be monitored using a substrate emission, e.g., Au 4f<sub>7/2</sub> in the case of Au. The Au 4f<sub>7/2</sub> spectra of the clean Au substrate in Figure 3 exhibit a splitting of the emission in two components at ≈83.95 and ≈83.65 eV, which can be assigned to the gold atoms in the bulk and topmost surface layer, respectively.<sup>34</sup> This assignment is supported by the intensity decrease of the surface component with increasing kinetic energy of the photoelectrons (see Figure 3) and by the good agreement of the observed surface core level shift of –0.31 eV with literature values.<sup>34,49–51</sup> Upon the adsorption of C12SeSeC12 on Au substrates, the surface components shifts to higher binding energy, merging with the bulk component, as illustrated by Figure 4, where the Au 4f<sub>7/2</sub> HRXPS spectra for clean gold and C12Se/Au are presented. Since both components in C12Se/Au are difficult to disentangle, a suitable fingerprint to describe the adsorbate-induced shift of the surface component is the fwhm of the joint Au 4f<sub>7/2</sub> emission. The values of this parameter for clean Au, C12Se/Au, and C12S/

**TABLE 1: Binding Energy Positions (eV) and fwhm's (eV; in brackets) of the Photoemission Peaks for C12Se, C12S, and C12SeC12 SAMs on Au and Ag**

	C12Se		C12S		C12SeC12	
	Au	Ag	Au	Ag	Au	Ag
C 1s, $h\nu=350$ eV	284.99 (0.82)	284.58 (0.89)	284.96 (0.83)	285.32 (0.77)	284.35 (1.1)	284.10 (1.2)
Se 3d or S 2p, $h\nu=150, 350$ eV	54.15 (0.74)	54.17 (0.51)	162.02 (0.52)	161.93 (0.60)	55.02 (0.61)	–

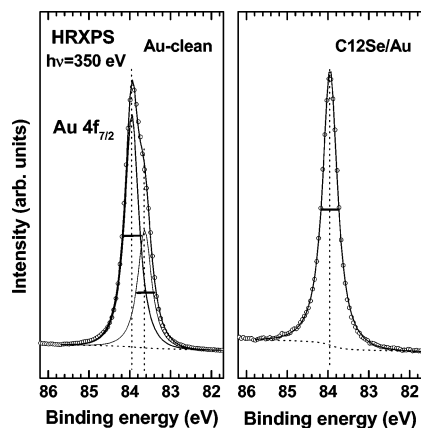


**Figure 4.** Normalized Au  $4f_{7/2}$  HRXPS spectra of clean Au and C12Se/Au acquired at a photon energy of 350 eV. The decomposition of the former spectrum into the bulk and surface components is shown.

**TABLE 2: fwhm's (eV) of the Au  $4f_{7/2,5/2}$  Components for Clean Au, C12Se/Au, and C12SAu**

system\photon energy	350 eV	580 eV
clean Au	0.405	0.424
C12Se/Au	0.432	0.440
C12S/Au	0.46	0.47

Au, where a similar shift of the Au  $4f_{7/2}$  surface component is observed,<sup>34</sup> are compiled in Table 2. The data for two different photon energies are presented; the higher fwhm value for the higher photon energy is related to increasing energy spreading of the primary photon beam. As seen in Table 2, the Au  $4f_{7/2}$  fwhm for C12Se/Au is somewhat smaller (by 0.03 eV) than that for C12S/Au, which suggests that the surface component shifts closer to the bulk component in the former case. Assuming the shift of 0.25 eV upon the adsorption of AT on Au,<sup>34</sup> one gets an adsorbate-induced shift of 0.28 eV for the Au  $4f_{7/2}$  surface component in the case of C12SeSeC12.

A similar analysis is more difficult in the case of the Ag substrate, since the surface core level shift for the clean Ag surface is much smaller than that for gold, so that the bulk and surface components are merged together.<sup>34</sup> However, some tentative conclusions can be derived from the Se 3d spectra. In the case of the C12Se films, the Se 3d doublet has almost identical BE positions on Au and Ag, whereas the BE position of the S 2p doublet in C12S/Ag is lower (by  $\approx 0.1$  eV) than that in C12S/Au (Table 1). A lower BE is indirect indication of a higher extent of the charge transfer, i.e., a stronger bond. Therefore, we may assume that the selenium–silver bond is weaker than the sulfur–silver one. Note, however, that this statement is only a tentative one, since the charge transfer is not the only parameter affecting the BE positions of the Se 3d and S 2p doublets. Another parameter, namely the final state effects due to conduction electrons of the substrates (see e.g. ref 52), should be considered in detail, which is rather difficult for the systems under considerations.

Along with the BE position of the Se 3d doublet, an important parameter is the fwhm of the Se  $3d_{5/2}$  and Se  $3d_{3/2}$  components. Since the instrumental spreading is negligible in the present case, the value of fwhm is characteristic of the inhomogeneity of the bonding configurations (e.g. the distribution of the adsorption sites) for the selenol headgroups. A noticeable larger Se  $3d_{5/2,3/2}$  fwhm for C12Se/Au as compared to C12Se/Ag suggests a larger inhomogeneity (e.g. a coexistence of several different adsorption sites) in the former case. This fwhm relation is just opposite to the case of C12S, where a larger fwhm is observed for Ag

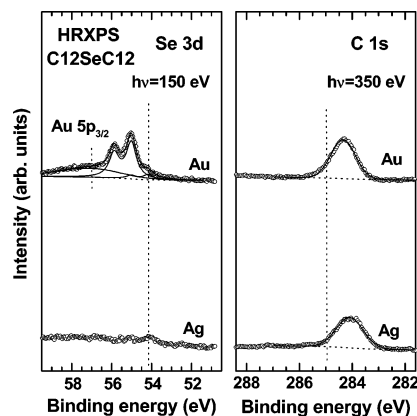


**Figure 5.** Normalized Se 3d and C 1s HRXPS spectra of C12SeC12/Au and C12SeC12/Ag (open circles) acquired at photon energies of 150 and 350 eV, respectively, along with the corresponding fits (solid lines). The same intensity scale as in Figure 1 is used. The BE positions of the Se  $3d_{5/2}$  component and C 1s emission for C12Se/Au (see Figure 1) are marked by the dotted lines as references. A background is shown.

**TABLE 3: Effective Thickness ( $\text{\AA}$ ) of the C12Se and C12S SAMs on Au and Ag**

	C12Se HRXPS	C12S HRXPS	C12Se ellipsometry	C12S ellipsometry
Au	14.5	14.9	14.6	14.7
Ag	13.9	15.6	—	—

substrate (see Figure 2 and Table 1), in accordance with the incommensurate  $(\sqrt{7} \times \sqrt{7})R19.1^\circ$  structure.<sup>2,4,7–9</sup>

The C 1s HRXPS spectra of C12Se/Au and C12Se/Ag in Figure 1 exhibit a single emission. The BE position of this emission for C12Se/Au (284.99 eV) is noticeably higher than that for C12Se/Ag (284.58 eV). This is distinctly different from the case of C12S: the BE position of the C 1s emission for C12S/Au (284.96 eV) is smaller than that for C12S/Ag (285.32 eV). The comparison of the values for the C12Se and C12S films shows that the BE position of the C 1s emission does not change significantly upon exchange of thiol for selenol on Au, but decreases by 0.74 eV on Ag.

Apart from the above consideration, the intensities of the C 1s emission could be evaluated. They were rather similar for C12Se/Au and C12Se/Ag, but quite different for C12S/Au and C12S/Ag, where a larger value is observed for Ag. Based on the exact values of C 1s intensity, and taking into account the intensities of the Au 4f and Ag 3d emissions, the thicknesses of the C12Se and C12S SAMs were determined from the  $I_{C1s}/I_{Au4f}$  and  $I_{C1s}/I_{Ag3d}$  ratios. The derived values are presented in Table 3, along with the ellipsometry data (see below). For the evaluation, the attenuation lengths reported in ref 53 were used. It can clearly be seen that the layers on Au must have a similar orientation, since the thicknesses are almost the same, while on Ag the thickness of the C12Se layer is considerably smaller than the C12S film, suggesting either a larger tilt and/or a looser packing of the former.

The results for the C12Se SAMs can be compared with those for the C12SeC12 films. Normalized Se 3d and C 1s HRXPS spectra of C12SeC12/Au and C12SeC12/Ag are presented in Figure 5, along with the corresponding fits. The results of fitting and a quantitative analysis of these spectra are compiled in Table 1. The Se 3d spectra of C12SeC12/Au are dominated by a Se  $3d_{5/2,3/2}$  doublet at a BE of 55.02 eV, which is characteristic of weakly bound Se and noticeably higher than the respective value for C12Se/Au (54.15 eV). There is only a weak intensity at the latter BE position in the spectra of C12SeC12/Au. This suggests

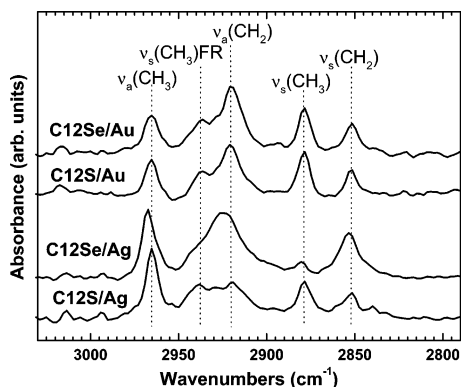


**Figure 6.** IRRAS spectra of the C12Se and C12S SAMs on Au and Ag. The characteristic absorption bands are indicated. The positions of these bands for C12S/Au are marked by the dotted lines as a guide for eye.

**TABLE 4: Positions (cm<sup>-1</sup>) of the C–H Stretching Modes in the IRRAS Spectra of C12Se, C12S, and C12SeC12 SAMs on Au and Ag (ip means in-plane)**

	$\nu_a(\text{CH}_3)$	$\nu_s(\text{CH}_3)\text{FR}$	$\nu_a(\text{CH}_2)$	$\nu_s(\text{CH}_3)$	$\nu_s(\text{CH}_2)$
TDM direction	$\perp$ C–CH <sub>3</sub> ip C–C–C	$\parallel$ C–CH <sub>3</sub>	$\perp$ C–C–C	$\parallel$ C–CH <sub>3</sub>	ip C–C–C ip H–C–H
C12S/Au	2965.5	2937.5	2920.3	2878.5	2852
C12S/Ag	2965.5	2937.5	2919.7	2878.5	2852
C12Se/Au	2965.5	2937.5	2919.7	2878.5	2852
C12Se/Ag	2967	2939	2924	2880.2	2853.5
C12SeC12/Au	2966	2937.5	2926.5	2880.5	2855.5

that the vast majority of the C12SeC12 species experiences no cleavage of one of the two C–Se bonds in C12SeC12 (leading to the formation of a gold selenolate) upon the adsorption on Au. Under these circumstances, a densely packed SAM cannot be formed, as evidenced by the C 1s HRXPS spectra of C12SeC12/Au, where a much lower intensity than for C12Se/Au (Figure 1) is observed. Also, the BE position of the C 1s emission in the spectra of C12SeC12/Au is noticeably lower than that for C12Se/Au. This can be related to the different structure of the C12SeC12 film and a higher extent of the substrate-mediated screening of the C 1s photoemission hole in the thinner C12SeC12/Au.

The situation for C12SeC12/Ag is even more abnormal. Almost no intensity is observed in the Se 3d spectrum, and there is only a weak emission in the C 1s spectra. The observed BE position (284.1 eV) is characteristic of carbon contamination. Presumably, the C12SeC12 molecules are not able to oust contamination from the Ag surface. Note, that the surface of the even freshly prepared Au and Ag substrates is contaminated to some extent because of their exposure to ambient. This contamination is, however, displaced upon SAM formation.<sup>2</sup>

**3.2. Ellipsometry.** The effective thicknesses of the C12Se and C12S films on Au derived from the ellipsometry measurements are presented in Table 3. These values agree fairly well with the thicknesses calculated on the basis of the HRXPS data. The ellipsometry measurements for the films on Ag were not performed.

**3.3. IRRAS.** IRRAS spectra of C12Se and C12S SAMs on Au and Ag are presented in Figure 6. All spectra exhibit characteristic asymmetric ( $\nu_a$ ) and symmetric ( $\nu_s$ ) C–H stretching bands of methyl and methylene (marked in the figure) and a Fermi-resonance band of methyl ( $\nu_s$  FR); the positions of these bands are compiled in Table 4. The positions of the asymmetric and symmetric methylene stretching bands in C12Se/Au, C12S/Au, and C12S/Ag are almost identical. The corresponding values are  $\approx 2920$  and  $\approx 2852$  cm<sup>-1</sup>, respectively. Such band positions are characteristic for crystalline-like packing of the alkyl chains.

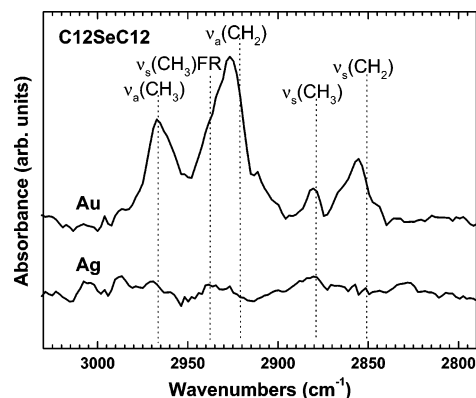


**Figure 7.** IRRAS spectra of C12SeC12/Au and C12SeC12/Ag. The characteristic absorption bands are indicated. The positions of these bands for C12Se/Au (see Figure 6) are marked by the dotted lines as references.

This suggests all-trans conformation of these chains with a very low concentration of gauche defects.<sup>13,43</sup> The positions of the asymmetric and symmetric methylene stretching bands in C12Se/Ag are somewhat higher, namely 2924 and 2853.5 cm<sup>-1</sup>, respectively (the methyl bands are shifted as well). In addition, these bands are broader than the analogous modes in the spectra of C12Se/Au, C12S/Au, and C12S/Ag. These differences indicate some gauche conformations around the C–C bonds in C12Se/Ag. Each gauche bond shifts the vibrational frequencies of the adjoining methylene groups by 10–20 wavenumbers. A liquid alkane at room temperature has  $\sim 40\%$  C–C gauche conformations and peak maxima at 2928 and 2856 cm<sup>-1</sup>.<sup>43</sup>

The relative intensities of the C–H stretching bands are very similar for C12Se/Au and C12S/Au, but somewhat different for C12Se/Ag and C12S/Ag (see e.g. the symmetric methyl and methylene stretching bands). Note that the ratio of the band intensities is a fingerprint of the molecular orientation in the SAMs and can even be used for extracting quantitative information on the film structure.<sup>54–56</sup> According to the selection rules for surface IR spectroscopy, only vibrational modes with the transition dipole moment (TDM) perpendicular to the surface can be excited. At an inclined orientation of the TDM, only its perpendicular component contributes to the absorbance, so that the orientation of the functional group can be determined if at least two orthogonal modes are considered. Such an analysis is, however, not necessary in our case, since we can get the structural information from the NEXAFS data. We only want to point out that, in view of the above consideration, the IRRAS results suggest similar orientations for C12Se/Au and C12S/Au, but different orientations for C12Se/Ag and C12S/Ag.

This difference is, however, not as significant as the difference between the SAMs formed from the dialkyl diselenides and dialkyl selenides. The IRRAS spectra of C12SeC12/Au and C12SeC12/Ag are presented in Figure 7. The spectra of C12SeC12/Au exhibit all characteristic C–H stretching modes of the methyl and methylene groups, but intensity relations between these modes are noticeably different from those for C12Se/Au. Also, the positions of the asymmetric and symmetric methylene stretching bands in C12SeC12/Au (2926.5 and 2855.5 cm<sup>-1</sup>, respectively) are somewhat higher than those in C12Se/Au (2919 and 2851 cm<sup>-1</sup>). Along with a significant broadening of the absorption peaks for C12SeC12/Au, this suggests a disordered structure with a high percentage of the gauche defects in the C12SeC12 film on Au. In the case of Ag, no characteristic modes of the methyl and methylene groups are observed, in full agreement with the HRXPS results. There is only carbon contamination on the Ag surface.

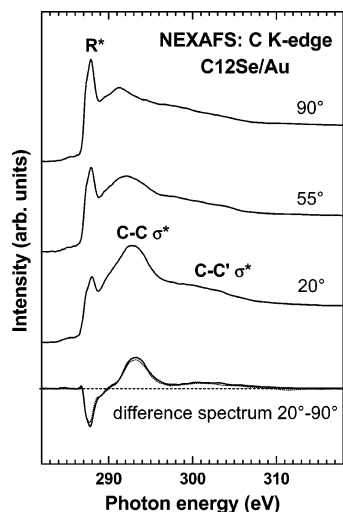


**Figure 8.** Carbon K-edge NEXAFS spectra of C12Se/Au acquired at X-ray incident angles of 90°, 55°, and 20°, along with the difference between the 90° and 20° spectra. For comparison, the analogous difference spectrum of C12S/Au is also given by the dotted line. It overlaps completely with the spectrum of C12Se/Au. The dashed line corresponds to zero. The characteristic absorption resonances are indicated.

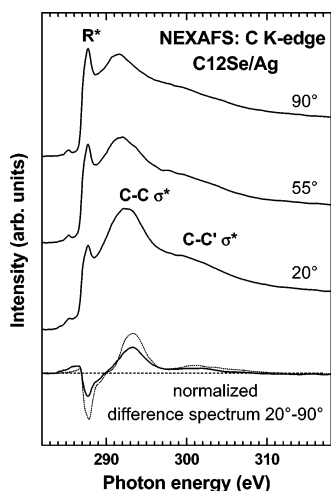


**Figure 9.** Carbon K-edge NEXAFS spectra of C12Se/Ag acquired at X-ray incident angles of 90°, 55°, and 20°, along with the difference between the 90° and 20° spectra. The difference spectrum is normalized to the R\* intensity ratio between the 55° spectra of C12Se/Ag and C12Se/Au, for direct comparison to the respective spectrum of C12Se/Au. For comparison, the analogous difference spectrum of C12S/Ag is also given by the dotted line. The dashed line corresponds to zero. The characteristic absorption resonances are indicated.

**3.4. NEXAFS.** In NEXAFS experiment, core level electrons (e.g. C1s for a C K-edge spectrum) are excited into nonoccupied molecular orbitals, which are characteristic for specific bonds, functional groups, or molecules. The PE positions of the respective absorption resonances give then a clear signature of these entities. In addition, information on molecular orientation can be derived from the experimental data, since the cross-section of the resonant photoexcitation process depends on the orientation of the electric field vector of the linearly polarized synchrotron light with respect to the molecular orbital of interest (so-called linear dichroism in X-ray absorption).<sup>57</sup>

Carbon K-edge NEXAFS spectra of C12Se/Au and C12Se/Ag acquired at X-ray incident angles of 90°, 55°, and 20° are presented in Figures 8 and 9, respectively, along with the difference between the 90° and 20° spectra for the C12Se and C12S SAMs. All spectra in Figures 8 and 9 exhibit a C1s

absorption edge related to C 1s  $\rightarrow$  continuum excitations and all characteristic absorption resonances of extended alkyl chains, namely a sharp resonance at  $\approx 287.7$  eV, and two broader resonances at  $\approx 293.4$  eV and  $\approx 301.6$  eV. The two latter resonances are commonly related to valence, antibonding C–C  $\sigma^*$  and C–C'  $\sigma^*$  orbitals,<sup>57,58</sup> while the resonance at 287.7 eV is alternatively attributed to the excitations into pure valence orbitals,<sup>57,59</sup> predominantly Rydberg states<sup>60,61</sup> and mixed valence/Rydberg states.<sup>62</sup> This resonance consists of several individual resonances, which are merged together.<sup>59–61</sup> We will denote it as a R\* resonance but take into account a possible admixture of antibonding C–H\* orbitals. The molecular orbitals related to the R\* resonance are supposed to be orientated perpendicular to the alkyl chains,<sup>58,63,64</sup> whereas the transition dipole moments of the orbitals corresponding to the C–C  $\sigma^*$  and C–C'  $\sigma^*$  resonances are believed to be directed along the chain axis.<sup>63</sup> Thus, the orientations of these orbitals unequivocally determine the orientation of the alkyl chains in the investigated films.

The NEXAFS spectra of C12Se/Au and C12Se/Ag in Figures 8 and 9 exhibit a pronounced linear dichroism, i.e., a dependence of the absorption resonance intensity on the incidence angle of X-rays, which suggests a high orientational order in these SAMs. Considering the TDM directions of the R\*, C–C  $\sigma^*$ , and C–C'  $\sigma^*$  orbitals and the character of the observed intensity changes, an upright orientation of the alkyl chains in C12Se/Au and C12Se/Ag can be assumed. A fingerprint of the orientational order and average molecular inclination is a difference spectrum.<sup>19,57</sup> Such spectra of C12Se/Au and C12S/Au in Figure 8 are almost identical, which suggest a comparable orientational order and similar molecular inclinations in both films. In contrast, the peak amplitudes in the difference spectrum of C12Se/Ag in Figure 9 are noticeably smaller than those in the spectrum of C12S/Ag, which imply a lower orientational order and/or a larger molecular inclination in C12Se/Ag.

Apart from these qualitative considerations, a quantitative analysis can be performed, and the average tilt angles of alkyl chains can be determined. For this purpose, the intensity of an absorption resonance  $I$  should be monitored as a function of the X-ray incidence angle  $\theta$  and the resulting dependence evaluated according to theoretical expression (for a plane-type orbital)<sup>57</sup>

$$I(\alpha, \theta) = A \{ P \times (2/3) [1 - (1/4) \cdot (3 \cdot \cos^2 \theta - 1) \cdot (3 \cdot \cos^2 \gamma - 1)] + (1 - P) \times (1/2) \cdot (1 + \cos^2 \gamma) \} \quad (1)$$

where  $A$  is a constant,  $P$  is a polarization factor of the X-rays, and  $\gamma$  is the angle between the sample normal and the normal of the molecular orbital plane.

For the evaluation, the R\* resonance as the most intense one in the spectra has been selected. The respective orbital was considered as a plane-type one. To avoid normalization problems, not the absolute intensities but the intensity ratios  $I(\theta)/I(90^\circ)$  were analyzed,<sup>57</sup> where  $I(\theta)$  and  $I(90^\circ)$  are the intensities of the R\* resonance at X-ray incidence angles of  $\theta$  and  $90^\circ$ . The angular dependences of the R\* resonance intensity ratio  $I(\theta)/I(90^\circ)$  for the C12Se films are presented in Figure 10, along with the best theoretical fits according to the eq 1. The derived values of the average tilt angles of the alkyl chains in C12Se/Au and C12Se/Ag are given at the respective fit curves; they are 28° and 37°, respectively. The accuracy of these values is  $\pm 3$ –5°, which is just a general accuracy of the NEXAFS experiment and data evaluation procedure. The value for C12Se/Au is very close to that for C12S/Au ( $\approx 30^\circ$ ), whereas the

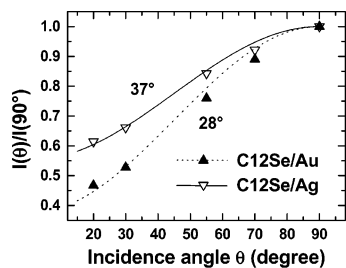


**Figure 10.** The angular dependence of the  $R^*$  resonance intensity ratio  $I(\theta)/I(90^\circ)$  for C12Se/Au (up filled triangles) and C12Se/Ag (down open triangles) along with the best theoretical fits according to eq 1 (dotted and solid lines, respectively). The derived tilt angles are given at the respective fit curves.

**TABLE 5: Advancing ( $\theta_{adv}$ ) and Receding ( $\theta_{rec}$ ) Water Contact Angles of the C12Se, C12S, and C12SeC12 SAMs on Au and Ag**

	C12Se		C12S		C12SeC12	
	$\theta_{adv}$	$\theta_{rec}$	$\theta_{adv}$	$\theta_{rec}$	$\theta_{adv}$	$\theta_{rec}$
Au	110°	101°	111°	102°	100°	89°
Ag	111°	102°	112°	101°	98°	75°

average tilt angles in C12Se/Ag is noticeably larger than that in C12S/Ag (12–15°).

**3.5. Contact Angle Measurements.** The values of the advancing ( $\theta_{adv}$ ) and receding ( $\theta_{rec}$ ) water contact angles of the C12Se, C12S, and C12SeC12 SAMs on Au and Ag are given in Table 5. The  $\theta_{adv}$  and  $\theta_{rec}$  values in the C12Se and C12S films are practically identical and characteristic of well-ordered AT SAMs with the CH<sub>3</sub> termination.<sup>44,65</sup> The difference between the advancing and receding contact angles, i.e., the contact angle hysteresis, is only 9–11° in these films, which suggest that their film–ambient interface is rather smooth.

The  $\theta_{adv}$  and  $\theta_{rec}$  values on the C12SeC12 films are noticeably smaller than those on the C12Se and C12S SAMs, and the contact angle hysteresis on Ag is very large (23°). This suggests a partial exposure of the CH<sub>2</sub> groups in C12SeC12/Au to the surface and a rather rough “film”–ambient interface in C12SeC12/Ag.

**3.6. C16SeSeC16.** Despite all our efforts and an extended variation of the parameters of the preparation procedure (solvent, the substance concentration, sonification, etc.), we have not succeeded to prepare high-quality C16Se SAMs on Au and Ag. Even though the IRRAS spectra were characteristic of crystalline alkylselenol SAMs, there were additional emissions except for the selenolate doublet in the Se 3d HRXPS spectra. At the moment, we cannot conclude whether there is a physical reason behind these difficulties or just a broader variation of the layer preparation parameters is required. We think that further work is necessary to clarify this issue.

#### 4. Discussion

All experimental data suggest that C12SeSeC12 form contamination-free, densely packed, and well-ordered C12Se SAMs on (111) Au and Ag substrates. The molecules are bound to the substrate via a selenolate–gold linkage, while the alkyl backbones have an upright orientation. The selenolate–gold linkage is formed after the cleavage of the Se–Se bond, which occur by an oxidative addition mechanism, upon the adsorption, similar to the formation of the thiolate bonds from the disulfide precursors.

The slightly larger shift of the Au 4f<sub>7/2</sub> surface component upon the adsorption of selenium as compared to sulfur suggests that the selenolate–gold bond is stronger than the thiolate–

gold one, even if insignificantly. This is in contrast with the intuitive suggestion by Samant et al.<sup>21</sup> but in accordance with the STM data by Dishner et al.,<sup>22</sup> the substitution experiments by Huang et al.,<sup>24</sup> and electrochemistry measurements by Sato and Mizutani.<sup>30</sup> In particular, in the experiments by Huang et al., it was observed that diphenyl diselenide (DPDSe) displaces benzenethiolate from gold, but diphenyl disulfide does not displace benzeneselenolate.<sup>24</sup> The adsorption of DPDSe was found to be more favorable by 0.7 kcal/mol,<sup>24</sup> which is rather small as compared to the sulfur–gold interaction energy in AT/Au (44 kcal/mol).<sup>66</sup>

The analysis of the Se 3d spectra suggests that the selenium–silver bond is weaker than the sulfur–silver one, even if insignificantly. This result is in accordance with the substitution experiments by Hun et al.,<sup>24</sup> in which the adsorption of benzenethiolates was favored over the benzeneselenolate adsorption. The respective difference in the free energy of adsorption was calculated to be 0.3 kcal/mol, which is, similar to the case of Au, small as compared to the energies of Ag–S and Ag–Se bonds in diatomic systems (51.9 and 48.4 kcal/mol, respectively).<sup>67</sup>

The differences in the binding energy and exact bonding configurations of selenium on Au and Ag cause some differences in the structure of the C12Se and C12S films on these substrates. The packing density, orientational order, and molecular inclination in C12Se/Au were found to be very similar to those in C12S/Au. This suggests the same bonding configurations, i.e., sp<sup>3</sup>, for both sulfur and selenium on Au. The only noticeable difference between C12Se/Au and C12S/Au is a superposition of different adsorption sites in C12Se/Au, which follows from the relatively large value of the Se 3d<sub>5/2,3/2</sub> fwhm. This conclusion is in excellent agreement with the recent STM data for the C10Se and C12Se SAMs on Au, which suggest the multiple binding sites for alkylselenolates on Au(111).<sup>29</sup>

Note that the headgroup hybridization cannot be exclusively associated with a definite adsorption site (e.g. a sp<sup>3</sup> hybridization with a 3-fold hollow site) since there is a second important contribution to the hybridization. It is the electronic structure of the substrate, governing a specific overlap of the headgroup’s orbitals with the frontier orbitals of the substrate. Thus, an sp<sup>3</sup> hybridization can be characteristic of both C12Se/Au and C12S/Au, even though the adsorption sites or their superposition might be different. Note, that recent studies favor a top adsorption site for AT/Au,<sup>68,69</sup> although previous results suggested either 3-fold hollow<sup>2,6,70</sup> or bridge<sup>71,72</sup> positions.

The obtained value (28°) of the average tilt angle of alkyl chains in C12Se/Au is markedly different from the value reported by Samant et al. (15°).<sup>21</sup> Note, however, that these authors determined the average tilt angle of alkyl chains in docosanethiol on Au as 12°, which is obviously wrong in view of a vast majority of all other studies on AT/Au (≈30°).<sup>10,13,14</sup> Thus the angle value reported for C12Se/Au by Samant et al. can be strongly underestimated, just in the same way as it occurred for the docosanethiol SAM.

In contrast to the case of Au, C12Se/Ag exhibits significantly lower packing density, a lower degree of the conformational and orientational order, and a larger molecular inclination than C12S/Ag. A possible explanation for this difference can be the difference in the bonding configurations of selenium and sulfur on silver, i.e., sp<sup>3</sup> and sp, respectively. The sp<sup>3</sup> hybridization will favor a larger inclination of the alkyl chains in C12Se/Ag, similar to C12Se/Au. An alternative explanation is the larger corrugation of the selenium–silver binding energy surface as compared to the sulfur–silver case. This assumption is in accord

with the narrow Se  $3d_{5/2,3/2}$  emissions for C12Se/Ag (Figure 1), which can be associated with a single adsorption site for the C12Se molecules on Ag. Note, that in the case of a strong corrugation of the headgroup—substrate binding energy surface, the headgroups will be pinned at the energetically favorable positions, so that the energy minimization in a SAM can only be achieved by a molecular tilt.<sup>2</sup>

An interesting finding is the difference in the BE position of the C1s emission in C12Se/Ag and C12S/Ag (284.58 and 285.32 eV, respectively; see Table 1). The high value for C12S/Ag is untypical for saturated hydrocarbons and noticeably larger than that for C12S/Au. It was related to the detailed molecular arrangement in the alkyl matrix of AT/Ag, resulting in a specific screening of the C 1s photoemission hole by intermolecular chain transfer.<sup>73</sup> It is then understandable that a change in the molecular arrangement, as it for example happens at going from C12S/Ag to C12Se/Ag, will be accompanied by a drastic decrease in the BE position of the C 1s emission.

Along with the results for dialkyl diselenides, we have found that dialkyl selenides do not form high-quality SAMs on Au and Ag substrates. The vast majority of the C12SeC12 molecules do not undergo cleavage of the C—Se bond, leading to the formation of a gold selenolate, upon the adsorption. As a result, steric constraints provided by both chain parts do not allow a dense molecular packing and a high orientational and conformational order. This occurs in the case of C12SeC12/Au, where a SAM-like film is formed, but with a low packing density and a conformational disorder. In the case of Ag, the C12SeC12 species are not capable to remove contamination from the Ag surface and no SAM-like film, even if a bad quality, is formed.

The observed behavior of dialkyl selenides agrees quite well with that of dialkyl sulfides. Even though there was a controversy concerning the properties of the latter systems,<sup>74–79</sup> recent studies state that the maximum coverage achieved with a dialkyl sulfide is considerably lower than that with ATs, and substantial amounts of contamination remain on the substrate.<sup>80</sup>

## 5. Conclusion

Self-assembled monolayers formed from didodecyl diselenide (C12SeSeC12) and didodecyl selenide (C12SeC12) on (111) Au and Ag substrates were characterized by HRXPS, ellipsometry, IRRAS, NEXAFS spectroscopy, and water contact angle measurements. A  $\mu\text{mol}$  concentration of the molecular precursors and ethanol as the solvent were found to be essential for the SAM quality. C12SeSeC12 was found to form contamination-free, densely packed, and well-ordered SAMs on both substrates, whereas the adsorption of C12SeC12 occurred only on Au and resulted in the formation of a SAM-like film with a low packing density and a conformational disorder. On Ag, no SAM-like film was formed, since C12SeC12 was not capable to remove contamination from the Ag surface. The difference in the adsorption behavior of C12SeSeC12 and C12SeC12 was related to the cleavage of the Se—Se bond and formation of a selenolate-metal bond in the former case, whereas no cleavage of the Se—C bond occurred in the latter case, which resulted in a low reactivity and steric constraints, even when the adsorption took place.

The properties of the C12Se SAMs were compared with those of the C12S films. The packing density, orientational order, and molecular inclination in C12Se/Au were found to be very similar to those in C12S/Au. In particular, the average tilt angle of aliphatic chains in C12Se/Au was found to be  $28^\circ$ . The results suggest the same  $sp^3$  bonding configurations, but different distributions of adsorption sites for sulfur and selenium on Au.

In contrast, C12Se/Ag exhibits significantly lower packing density, a lower degree of the conformational and orientational order, and the larger molecular inclination than C12S/Ag. In particular, the average tilt angle of aliphatic chains in C12Se/Ag was found to be  $37^\circ$ . The difference between C12Se/Ag and C12S/Ag was tentatively explained by the difference in the bonding configurations of selenium and sulfur on silver, which are assumed to be  $sp^3$  and  $sp$ , respectively. Alternatively, a larger corrugation of the selenium—silver binding energy surface as compared to the sulfur—silver case can be assumed. The analysis of the experimental data suggests that the selenium—gold bond is stronger than the sulfur—gold one, whereas the inverse relation takes place for silver.

In addition to the C12Se and C12SeC12 films, SAMs formed from dihexadecyl diselenide have been studied. So far, the results are not completely convincing, and further work is necessary.

**Acknowledgment.** We thank M. Grunze for the support of this work, Thimo Bastuck for the help with the ellipsometry measurements, Ch. Wöll (Universität Bochum) for providing us with the experimental equipment for the NEXAFS measurements, L. S. O. Johansson (Karlstad University) for the cooperation at MAX-lab, and the BESSY II and MAX-lab staff for the assistance during the synchrotron-based experiments. This work has been supported by the German BMBF (05KS4VHA/4), European Community (Access to Research Infrastructure action of the Improving Human Potential Programme), and the Fonds der Chemischen Industrie. A.U. thanks the NSF for partial support through the MRSEC for Polymers at Engineered Interfaces.

## References and Notes

- (1) Ulman, A. *An Introduction to Ultrathin Organic Films: Langmuir–Blodgett to Self-Assembly*; Academic Press: New York, 1991.
- (2) Ulman, A. *Chem. Rev.* **1996**, *96*, 1533.
- (3) Ulman, A., Ed. *Thin films: self-assembled monolayers of thiols*; Academic Press: San Diego, CA, 1998.
- (4) Schreiber, F. *Prog. Surf. Sci.* **2000**, *65*, 151.
- (5) Schreiber, F. *J. Phys.: Condens. Matter.* **2004**, *16*, R881.
- (6) Sellers, H.; Ulman, A.; Shnidman, Y.; Eilers, J. E. *J. Am. Chem. Soc.* **1993**, *115*, 9389.
- (7) Ulman, A.; Eilers, J. E.; Tillman, N. *Langmuir* **1989**, *5*, 1147.
- (8) Fenter, P.; Eisenberger, P.; Li, J.; Camillone, N., III; Bernasek, S.; Scoles, G.; Ramanarayanan, T. A.; Liang, K. S. *Langmuir* **1991**, *7*, 2013.
- (9) Rieley, H.; Kendall, G. K.; Jones, R. G.; Woodruff, P. *Langmuir* **1999**, *15*, 8856.
- (10) Fenter, P.; Eisenberger, P.; Liang, K. S. *Phys. Rev. Lett.* **1993**, *70*, 2447; Fenter, P.; Eberhardt, A.; Eisenberger, P. *Science* **1994**, *266*, 1216.
- (11) Poirier, G. E.; Tarlov, M. J. *Langmuir* **1994**, *10*, 2853.
- (12) Thome, J.; Himmelhaus, M.; Zharnikov, M.; Grunze, M. *Langmuir* **1998**, *14*, 7435.
- (13) Nuzzo, R. G.; Dubois, L. H.; Allara, D. L. *J. Am. Chem. Soc.* **1990**, *112*, 558.
- (14) Laibinis, P. E.; Whitesides, G. M.; Allara, D. L.; Tao, Y.-T.; Parikh, A. N.; Nuzzo, R. G. *J. Am. Chem. Soc.* **1991**, *113*, 7152.
- (15) Walczak, M. M.; Chung, C.; Stole, S. M.; Widrig, C. A.; Porter, M. D. *J. Am. Chem. Soc.* **1991**, *113*, 2370.
- (16) Zharnikov, M.; Frey, S.; Rong, H.; Yang, Y. J.; Heister, K.; Buck, M.; Grunze, M. *Phys. Chem. Chem. Phys.* **2000**, *2*, 3359.
- (17) Frey, S.; Heister, K.; Zharnikov, M.; Grunze, M.; Tamada, K.; Colorado, R., Jr.; Graupe, M.; Shmakova, O. E.; Lee, T. R. *Isr. J. Chem.* **2000**, *40*, 81.
- (18) Rong, H. T.; Frey, S.; Yang, Y. J.; Zharnikov, M.; Buck, M.; Wühn, M.; Wöll, Ch.; Helmchen, G. *Langmuir* **2001**, *17*, 1582.
- (19) Zharnikov, M.; Grunze, M. *J. Phys. Condens. Matter.* **2001**, *13*, 11333.
- (20) Shaporenko, A.; Brunnbauer, M.; Terfort, A.; Grunze, M.; Zharnikov, M. *J. Phys. Chem. B* **2004**, *108*, 14462.
- (21) Samant, M. G.; Brown, C. A.; Gordon, J. G., II. *Langmuir* **1992**, *8*, 1615.

- (22) Dishner, M. H.; Hemminger, J. C.; Feher, F. J. *Langmuir* **1997**, *13*, 4788.
- (23) Bandyopadhyay, K.; Vijayamohan, K. *Langmuir* **1998**, *14*, 625.
- (24) Huang, F. K.; Horton, R. C., Jr.; Myles, D. C.; Myles, D. C.; Garrell, R. L. *Langmuir* **1998**, *14*, 4802.
- (25) Bandyopadhyay, K.; Vijayamohan, K.; Venkataraman, M.; Pradeep, T. *Langmuir* **1999**, *15*, 5314.
- (26) Nakano, K.; Sato, T.; Tazaki, M.; Takagi, M. *Langmuir* **2000**, *16*, 2225.
- (27) Yee, C. K.; Ulman, A.; Ruiz, J. D.; Parikh, A.; White, H.; Rafailovich, M. *Langmuir* **2003**, *19*, 9450.
- (28) Han, S. W.; Lee, S. J.; Kim, K. *Langmuir* **2001**, *17*, 6981.
- (29) Monnell, J. D.; Stapleton, J. J.; Jackiw, J. J.; Dunbar, T.; Reinert, W. A.; Dirk, S. M.; Tour, J. M.; Allara, D. L.; Weiss, P. S. *J. Phys. Chem. B* **2004**, *108*, 9834.
- (30) Sato, Y.; Mizutani, F. *Phys. Chem. Chem. Phys.* **2004**, *6*, 1328.
- (31) Hu, X.; Tian, Z.; Lu, X.; Chen, Y. *Synth. Commun.* **1997**, *27*, 553.
- (32) Ruan, M.-D.; Zhao, H.-R.; Fan W.-Q.; Zhou X.-J.; *J. Organomet. Chem.* **1995**, *485*, 19.
- (33) Köhn, F. Diploma Thesis, Universität Heidelberg, Heidelberg, Germany, 1998.
- (34) Heister, K.; Zharnikov, M.; Grunze, M.; Johansson, L. S. O. *J. Phys. Chem. B* **2001**, *105*, 4058.
- (35) Wirde, M.; Gelius, U.; Dunbar, T.; Allara, D. L. *Nuc. Instrum. Methods Phys. Res. B* **1997**, *131*, 245.
- (36) Jäger, B.; Schürmann, H.; Müller, H. U.; Himmel, H.-J.; Neumann, M.; Grunze, M.; Wöll, Ch. *Z. Phys. Chem.* **1997**, *202*, 263.
- (37) Heister, K.; Zharnikov, M.; Grunze, M.; Johansson, L. S. O.; Ulman, A. *Langmuir* **2001**, *17*, 8.
- (38) Zharnikov, M.; Grunze, M. *J. Vac. Sci. Technol. B* **2002**, *20*, 1793.
- (39) *Surface chemical analysis – X-ray photoelectron spectrometers – Calibration of the energy scales*, ISO 15472, 2001.
- (40) Moulder, J. F.; Stickle, W. E.; Sobol, P. E.; Bomben, K. D. *Handbook of X-ray Photoelectron Spectroscopy*, Chastian, J., Ed.; Perkin-Elmer Corp.: Eden Prairie, MN, 1992.
- (41) Zharnikov, M.; Frey, S.; Heister, K.; Grunze, M. *Langmuir* **2000**, *16*, 2697.
- (42) Batson, P. E. *Phys. Rev. B* **1993**, *48*, 2608.
- (43) Porter, M. D.; Bright, T. B.; Allara, D. L.; Chidsey, C. E. D. *J. Am. Chem. Soc.* **1987**, *109*, 3559.
- (44) Laibinis, P. E.; Bain, C. D.; Nuzzo, R. G.; Whitesides, G. M. *J. Phys. Chem.* **1995**, *99*, 7663.
- (45) Bain, C. D.; Biebuyck, H. A.; Whitesides, G. M. *Langmuir* **1989**, *5*, 723.
- (46) Beamson, G.; Briggs, D. *High-Resolution XPS of Organic Polymers*, John Wiley & Sons: Chichester, 1995.
- (47) Nuzzo, R. G.; Zegarski, B. R.; Dubois, L. H. *J. Am. Chem. Soc.* **1997**, *119*, 7733.
- (48) Bensebaa, F.; Zhou, Yu.; Deslandes, Y.; Kruus, E.; Ellis, T. H. *Surf. Sci.* **1998**, *405*, L472.
- (49) Culbertson, R. J.; Feldman, L. C.; Silverman, P. J.; Boehm, H. *Phys. Rev. Lett.* **1981**, *47*, 675.
- (50) Citrin, P. H.; Wertheim, G. K.; Baer, Y. *Phys. Rev. B* **1983**, *27*, 3160.
- (51) Hsieh, T. C.; Shapiro, A. P.; Chiang, T.-C. *Phys. Rev. B* **1985**, *31*, 2541.
- (52) Shaporenko, A.; Adlkofer, K.; Johansson, L. S. O.; Ulman, A.; Grunze, M.; Tanaka, M.; Zharnikov, M. *J. Phys. Chem. B* **2004**, *108*, 17964.
- (53) Lamont, C. L. A.; Wilkes, J. *Langmuir* **1999**, *15*, 2037.
- (54) Debe, M. K. *J. Appl. Phys.* **1984**, *55*, 3354.
- (55) Allara, D. L.; Nuzzo, R. G. *Langmuir* **1985**, *1*, 51.
- (56) Parikh, A. N.; Allara, D. L. *J. Chem. Phys.* **1992**, *96*, 927.
- (57) Stöhr, J. *NEXAFS Spectroscopy*; Springer Series in Surface Science 25, Springer-Verlag: Berlin, 1992.
- (58) Outka, D. A.; Stöhr, J.; Rabe, J. P.; Swalen, J. D. *J. Chem. Phys.* **1988**, *88*, 4076.
- (59) Schöll, A.; Fink, R.; Umbach, E.; Mitchell, G. E.; Urquhart, S. G.; Ade, H. *Chem. Phys. Lett.* **2003**, *370*, 834.
- (60) Bagus, P. S.; Weiss, K.; Schertel, A.; Wöll, Ch.; Braun, W.; Hellwig, H.; Jung, C. *Chem. Phys. Lett.* **1996**, *248*, 129.
- (61) Weiss, K.; Bagus, P. S.; Wöll, Ch. *J. Chem. Phys.* **1999**, *111*, 6834.
- (62) Väterlein, P.; Fink, R.; Umbach, E.; Wurth, W. *J. Phys. Chem.* **1998**, *108*, 3313.
- (63) Hähner, G.; Kinzler, M.; Wöll, Ch.; Grunze, M.; Scheller, M.; Cederbaum, L. S. *Phys. Rev. Lett.* **1991**, *67*, 851; *Phys. Rev. Lett.* **1992**, *69*, 694 (erratum).
- (64) Hähner, G.; Kinzler, M.; Thümmel, C.; Wöll, Ch.; Grunze, M. *J. Vac. Sci. Technol.* **1992**, *10*, 2758.
- (65) Laibinis, P. E.; Whitesides, G. M. *J. Am. Chem. Soc.* **1992**, *114*, 1990.
- (66) Dubois, L. H.; Nuzzo, R. G. *Ann. Phys. Chem.* **1992**, *43*, 437.
- (67) Smoes, S.; Mandy, F.; Vander Auwera-Mahieu, A.; Drowart, J. *Bull. Soc. Chim. Belg.* **1972**, *81*, 45.
- (68) Kondoh, H.; Iwasaki, M.; Shimada, T.; Amemiya, K.; Yokoyama, T.; Ohta, T.; Shimomura, M.; Kono, S. *Phys. Rev. Lett.* **2003**, *90*, 066102–1.
- (69) Roper, M. G.; Skegg, M. P.; Fisher, C. J.; Lee, J. J.; Dhanak, V. R.; Woodruff, D. P.; Jones, R. G. *Chem. Phys. Lett.* **2004**, *389*, 87.
- (70) Grönbeck, H.; Curioni, A.; Andreoni, W. *J. Am. Chem. Soc.* **2000**, *122*, 3839.
- (71) Vargas, M. C.; Giannozzi, P.; Selloni, A.; Scoles, G. *J. Phys. Chem. B* **2001**, *105*, 9509.
- (72) Hayashi, T.; Morikawa, Y.; Nozoye, H. *J. Chem. Phys.* **2001**, *114*, 7615.
- (73) Heister, K.; Johansson, L. S. O.; Grunze, M.; Zharnikov, M. *Surf. Sci.* **2003**, *529*, 36.
- (74) Sandroff, C. J.; Herschbach, D. R. *J. Phys. Chem.* **1982**, *86*, 3277.
- (75) Troughton, B.; Bain, C. D.; Whitesides, G. M. *Langmuir* **1988**, *4*, 365.
- (76) Bain, C. D.; Whitesides, G. M. *J. Phys. Chem.* **1989**, *93*, 1670.
- (77) Lee, S. B.; Kim, K.; Kim, M. S. *J. Phys. Chem.* **1992**, *96*, 9940.
- (78) Zhang, M.; Anderson, M. R. *Langmuir* **1994**, *10*, 2807.
- (79) Zhong, C. J.; Porter, M. D.; *J. Am. Chem. Soc.* **1994**, *116*, 11616.
- (80) Jung, Ch.; Dannenberger, O.; Xu, Y.; Buck, M.; Grunze, M. *Langmuir* **1998**, *14*, 1103.